

PAPER • OPEN ACCESS

## Characterising the area under the curve loss function landscape

To cite this article: Maximilian P Niroomand *et al* 2022 *Mach. Learn.: Sci. Technol.* **3** 015019

View the [article online](#) for updates and enhancements.

### You may also like

- [Orbital-selective Mottness in layered iron oxychalcogenides: the case of  \$\text{Na}\_x\text{Fe}\_2\text{OSe}\_2\$](#)   
L Craco, M Š Laad and S Leoni
- [On the capacity and superposition of minima in neural network loss function landscapes](#)  
Maximilian P Niroomand, John W R Morgan, Conor T Cafolla et al.
- [Review on experimental and theoretical investigations of the early stage, femtoseconds to microseconds processes during laser ablation in liquid-phase for the synthesis of colloidal nanoparticles](#)  
A Kanitz, M-R Kalus, E L Gurevich et al.



## PAPER

## Characterising the area under the curve loss function landscape

## OPEN ACCESS

Maximilian P Niroomand\* , Conor T Cafolla, John W R Morgan and David J Wales\* 

Department of Chemistry University of Cambridge, Cambridge CB2 1EW, United Kingdom

\* Authors to whom any correspondence should be addressed.

E-mail: [mpn26@cam.ac.uk](mailto:mpn26@cam.ac.uk) and [dw34@cam.ac.uk](mailto:dw34@cam.ac.uk)

## RECEIVED

10 November 2021

## REVISED

4 January 2022

## ACCEPTED FOR PUBLICATION

10 January 2022

## PUBLISHED

21 January 2022

**Keywords:** area under the curve, loss function landscape, basin hopping, alternative loss function, loss function

Original Content from this work may be used under the terms of the [Creative Commons Attribution 4.0 licence](https://creativecommons.org/licenses/by/4.0/).

Any further distribution of this work must maintain attribution to the author(s) and the title of the work, journal citation and DOI.

**Abstract**

One of the most common metrics to evaluate neural network classifiers is the area under the receiver operating characteristic curve (AUC). However, optimisation of the AUC as the loss function during network training is not a standard procedure. Here we compare minimising the cross-entropy (CE) loss and optimising the AUC directly. In particular, we analyse the loss function landscape (LFL) of approximate AUC (appAUC) loss functions to discover the organisation of this solution space. We discuss various surrogates for AUC approximation and show their differences. We find that the characteristics of the appAUC landscape are significantly different from the CE landscape. The approximate AUC loss function improves testing AUC, and the appAUC landscape has substantially more minima, but these minima are less robust, with larger average Hessian eigenvalues. We provide a theoretical foundation to explain these results. To generalise our results, we lastly provide an overview of how the LFL can help to guide loss function analysis and selection.

**1. Introduction**

The area under the curve of the receiver operating characteristic curve (AUC) is a commonly used method to evaluate the accuracy and reliability of a neural network classifier. However, for mathematical reasons, the AUC cannot be used as the loss function to be minimised during neural network training (Menon and Elkan 2011). Instead, other functions such as cross-entropy are commonly employed. The stepwise nature of the AUC function is the reason that it is non-differentiable and hence cannot simply be optimised. However, the AUC can be approximated using surrogate losses such as the sigmoid function. This approach can lead to a formulation equivalent to the soft-AUC described by Calders and Jaroszewicz (2007), which is referred to here as appAUC. We find it intuitive to optimise a function that is as close as possible to the one used to evaluate the model. Our main contributions in this paper are therefore:

- To understand the use of different approximation to the AUC as the loss function employed in training of a neural network.
- To explore the organisation of the appAUC landscape and compare it to a 'standard' cross-entropy landscape.
- A theoretical foundation of the differences between appAUC and cross-entropy landscapes.
- To outline how a loss function landscape analysis can be useful for loss function selection.

To better understand the advantages and disadvantages of the approximated AUC loss function, we study the functional space, commonly referred to as LFL, using tools from the theoretical study of energy landscapes in molecular and condensed matter systems (Wales 2003). The usefulness of the energy landscape approach has previously been demonstrated in the context of neural network LFLs (Ballard *et al* 2017). We will employ methods from this approach to gain insights about geometric features of the LFL, including the number of minima, their curvatures, and their connectivity. By repeatedly surveying large parts of the LFL, we are, with high probability, able to find the true global minimum. Additionally, due to a Metropolis criterion in the global optimisation approach described below, we do not get stuck in a local minimum, and explore the full LFL, hence learning more about the functional surface. Instead of a single minimum, we aim to find a large number of minima that, together with transition states, provide a faithful coarse-grained

representation of the loss function landscape. We believe that this approach will yield valuable insights into the use of appAUC as a loss function in neural networks.

Various interesting questions arise from the use of an appAUC loss function. Besides a comparison of properties between landscapes, and the effects of hyperparameter changes, we are especially interested in the differences between appAUC and CE landscapes. Both loss functions, for the same neural network architecture, address the learning problem of finding a mapping  $f$  from input data to class label. Does this common foundation imply that minima of the CE loss function are also minima of the appAUC function, or are they at least very similar to each other? We will show below that this condition does not hold, and explain why. Furthermore, to the best of our knowledge, there has been no previous research into the functional properties of AUC surrogates. We believe that quantifying inherent, geometric properties of loss functions will provide a more fundamental understanding of the applicability of particular loss functions to distinct machine learning problems.

### 1.1. Related work

This contribution lies at the intersection of three different areas of research: general understanding and study of loss functions, the appAUC loss function in particular, and the study of loss function landscapes to understand neural networks. Optimising the AUC as a loss function has been considered before (Cortes and Mohri 2004). It has been shown that testing AUC is improved when a loss function is chosen that is closer to the true AUC function (Yan *et al* 2003). Nonetheless, optimising loss functions that approximate the AUC is rarely considered. One reason for this situation may be that the computational complexity is formally  $\mathcal{O}(N^2)$ , or specifically in the binary classification case employed here,  $\mathcal{O}(N_p N_N)$  where  $N_p$  are the positive data points and  $N_N$  the negative ones. Other reasons include the non-convexity and perceived complexity of the appAUC landscape, and importantly the fact that it has zero derivatives almost everywhere (Ghanbari and Scheinberg 2018). The loss function is one of the most critical choices in the design of a neural network, because it is the element that underlies the entire learning procedure. At first glance, it may appear that all loss functions solve the same problem for a given neural network, which led Rosasco *et al* (2004) to question the practical differences between alternative loss functions. Yet, it is widely accepted that different loss functions allow us to optimise for specific properties (Janocha and Czarnecki 2017). By studying the appAUC LFL, we can quantitatively address these important questions.

The topology of the loss function has been a topic of interest for over 20 years (Hochreiter and Schmidhuber 1997). Understanding the loss function for a given neural network can help to establish the fundamental interpretation of the ‘black-box’, as such networks are often described (Li *et al* 2017). However, a key problem with studying the LFL is the large associated computational cost. Unlike the standard machine learning approach, where only a single minimum is located, the LFL approach attempts to sample a representative set of minima, which may often exceed 10 000 solutions (Ballard *et al* 2017). Computing the true number of minima for a loss function would require enhanced sampling techniques (Wales 2013, Martiniani *et al* 2016).

Recently, others have looked into the LFL of overparameterised neural networks (Cooper 2018) and shown that various properties can be exploited to improve accuracy and, importantly, robustness of neural networks (Chaudhari *et al* 2019, Baldassi *et al* 2020). Insights from the LFL have also been used to understand initialisation methods and their relative success (Fort and Scherlis 2019). However, to the best of our knowledge, there has been no research so far into interpreting individual loss functions from the underlying LFL. In this work, we aim to address this knowledge gap, and show that studying the LFL can provide important insights into our understanding and design of neural networks and the associated loss functions.

## 2. Methods

### 2.1. Neural network

For this initial survey, we consider neural networks with a single hidden layer. We denote the set of data points as  $\mathcal{D} = (\mathbf{X}, \mathbf{c})$ , containing  $N := |\mathcal{D}|$  elements. For a given classification problem with  $C$  classes, a data point  $d \in \mathcal{D}$  has input features  $\mathbf{x}^d$ , and a known output class,  $c^d$ . We use a nonlinear tanh activation function and convert output values  $y_i$ ,  $i \in C$  into softmax probabilities by  $p_i(\mathbf{W}; \mathbf{x}^d) = \exp[y_i(\mathbf{W}; \mathbf{x}^d)] / \sum_{j=1}^C \exp[y_j(\mathbf{W}; \mathbf{x}^d)]$ , where  $\mathbf{W}$  denotes the weight vector containing all weights of the neural network. As a reference to compare with our appAUC loss function, we use a cross-entropy (CE) loss function, defined as:

$$\text{CE}(\mathbf{W}; \mathbf{X}) = -\frac{1}{N} \sum_{d=1}^N \ln(p_{c^d}(\mathbf{W}; \mathbf{x}^d)) + \lambda \mathbf{W}^2. \quad (1)$$

The  $\lambda \mathbf{W}^2$  in equation (1) represents an L2 regularisation term, which eliminates zero Hessian Eigenvalues and counteracts overfitting. We fix  $\lambda = 10^{-5}$  for a fair comparison between loss functions.

**2.2. Area under the curve**

To evaluate a model such as the one described above, it is standard practice to consider the receiver operating characteristic (ROC) and calculate the area under the curve (AUC) (Hastie et al 2009). For a given classifier, the ROC is a plot of the true positive ratio,  $T(P)$ , against the false positive ratio,  $F(P)$ . These quantities are defined by:

$$T(\mathbf{W}; \mathbf{X}, P) = \frac{\sum_{d=1}^N \delta(c^d - 1) \Theta(p_1(\mathbf{W}; \mathbf{x}^d) - P)}{\sum_{d=1}^N \delta(c^d - 1)}, \tag{2}$$

$$F(\mathbf{W}; \mathbf{X}, P) = \frac{\sum_{d=1}^N (1 - \delta(c^d - 1)) \Theta(p_1(\mathbf{W}; \mathbf{x}^d) - P)}{\sum_{d=1}^N 1 - \delta(c^d - 1)}, \tag{3}$$

where  $\delta(c^d - 1)$  is the Dirac delta function, and  $\Theta(p_1 - P)$  is the Heaviside step function, defined as

$$\delta(c^d - 1) = \begin{cases} 1 & \text{if } c^d = 1, \\ 0 & \text{if } c^d \neq 1, \end{cases} \quad \Theta(p_1 - P) = \begin{cases} 1 & \text{if } p_1 \geq P, \\ 0 & \text{if } p_1 < P, \end{cases} \tag{4}$$

and  $P$  is a parameter, which acts as a cutoff probability for the neural network to predict that a given data point belongs to class 1 ( $p_1$ ). Note that the choice of class 1 as a positive reading is arbitrary, and for a multi-class system, any class may be chosen.

The ROC curve is defined by  $T$  and  $F$  as  $P$  varies from 0 to 1. For a perfect classifier, the ROC would simply be a horizontal line at  $T = 1$  (i.e.  $\forall P \neq 0, T(P) = 1$ ), and the area under the curve would then be 1. The AUC is therefore a measure of how close the model is to a perfect classifier. Formally, the AUC as a function of network weights  $\mathbf{W}$ , parameterised by the data  $\mathbf{X}$ , is given by:

$$\text{AUC} = \int_0^1 T(\mathbf{W}; \mathbf{X}, P) dF(\mathbf{W}; \mathbf{X}, P) = \frac{1}{N_p N_n} \sum_p \sum_n \Theta(p_1(\mathbf{W}; \mathbf{x}^p) - p_1(\mathbf{W}; \mathbf{x}^n)), \tag{5}$$

where  $p$  labels positive data points (class 1), and  $n$  labels negative data points (not in class 1).

**2.3. Approximated AUC: appAUC loss function**

Most optimisation routines benefit from analytical derivatives of the function to be optimised. The function defined in equation (1) has smooth analytical derivatives, but equation (5) does not, because of the discontinuous step function. However, in a similar way to other approaches (e.g. (Calders and Jaroszewicz 2007)), one can replace the discontinuous  $\Theta$  function with an approximate, smooth, analytical surrogate function, which can then be differentiated and optimised. We write

$$\text{AUC}(\mathbf{W}; \mathbf{X}) \approx A(\mathbf{W}; \mathbf{X}) \equiv \frac{1}{N_p N_n} \sum_p \sum_n \frac{1}{1 + \exp(-\beta(p_1(\mathbf{W}; \mathbf{x}^p) - p_1(\mathbf{W}; \mathbf{x}^n)))}, \tag{6}$$

where the Heaviside step function has been replaced with a smooth sigmoid function:

$$\Theta(z) \rightarrow \sigma(z) \equiv \frac{1}{1 + \exp(-\beta z)}, \tag{7}$$

with parameter  $\beta$  that is discussed in detail in the [appendix](#). An important consideration for surrogate AUC loss functions is that they do not change the optimal solution when replacing the step function. Such surrogates are referred to as AUC-consistent (Agarwal 2014). Charoenphakdee et al (2019) show that sigmoid is an AUC-consistent surrogate. The appAUC loss function in equation (6) is now differentiable and can hence be used for optimisation, where we minimise the negative form of equation (6) such that a minimum (i.e. lower loss) is a good solution of higher AUC. For reference, we have included the analytical first and second derivatives for equation (6) in the [appendix](#).

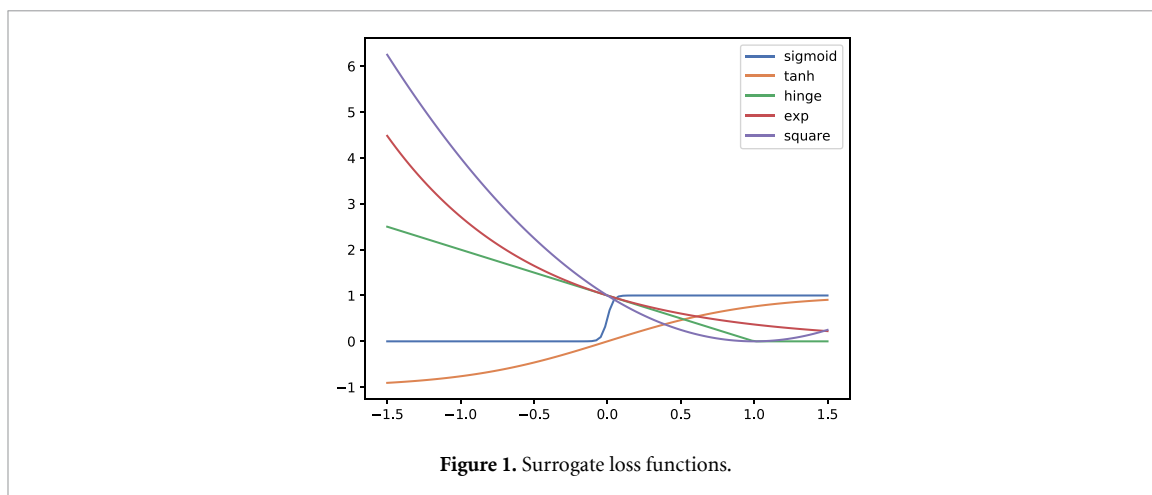


Figure 1. Surrogate loss functions.

### 2.3.1. Other surrogate loss functions

There exist many possible ways to approximate the AUC. Besides the sigmoid (equation (7)), we also show results for the popular (Gao and Zhou 2015) hinge  $\ell(z) = \max(0, 1 - z)$ , exponential  $\ell(z) = \exp(-z)$ , quadratic  $\ell(z) = (1 - z)^2$  and tanh surrogates (figure 1), where  $z$  denotes the difference in probability between true and false class i.e.  $P_T - P_N$ . Note that for the sigmoid in figure 1, we use  $\beta = 40$  (appendix). It is important to note that all but the hinge loss are AUC-consistent (Gao and Zhou 2015, Charoenphakdee *et al* 2019). AUC-consistency implies that the optimal solution remains unchanged with the surrogate loss replacing the true AUC. These different losses can all be used as surrogates because they include a pairwise comparison of positive and negative case probabilities as for the AUC.

## 2.4. Optimisation routines

Surveying the LFL for a neural network requires methods to locate minima of the landscape and connect them via transition states, defined as index one saddles (Murrell and Laidler 1968). We perform global optimisation using the basin-hopping method, which uses a Metropolis criterion to avoid getting stuck in local minima (Li and Scheraga 1987, Wales and Doye 1997). Further details regarding landscape exploration using basin-hopping are included in the appendix. We use a modified quasi-Newton L-BFGS minimiser (Nocedal 1980). Connectivity between minima is defined by transition states using a doubly-nudged (Trygubenko and Wales 2004a, 2004b) elastic band (Henkelman *et al* 2000, Henkelman and Jónsson 2000) approach and hybrid-eigenvector following (Munro and Wales 1999, Zeng *et al* 2014). These methods are implemented in the GMIN (Wales 1997), OPTIM (Wales 2003) and PATHSAMPLE (Wales 2003) programs, which are available for use under the GNU GPL.

## 2.5. Disconnectivity graphs

To visualise the high-dimensional loss function landscape, we employ disconnectivity graphs (Becker and Karplus 1997, Wales *et al* 1998), which provide a characteristic representation of the organisation for a high-dimensional surface. The vertical axis corresponds to increasing loss value, highlighting the barrier heights between local minima, and the horizontal arrangement is chosen to avoid crossings between the branches. In molecular science the vertical axis corresponds to potential or free energy, so the loss value plays the role of the energy in the LFL. Any node at which two or more branches split up can be understood as the minimum energy (loss) required for the system to move between the sets of minima associated with the respective branches. Such points correspond to the energies of transition states, discretised at a regular set of threshold values. Each leaf (tip) of the graph corresponds to a minimum of the LFL; the lower the leaf is, the lower its loss value. The lowest-lying leaf is the global minimum. Disconnectivity graphs provide a concise and intuitive way to visualise complex topologies, and preserve a faithful representation of the barriers on the landscape.

## 2.6. Dataset

The LFL is not only a function of the weights, but also of the data, as shown in equation (6). We will present our analysis of the AUC landscape mostly using the synthetic spiral dataset, introduced by Lang and Witbrock (1988). Spiral data remains one of the most popular synthetic datasets due to its high degree of non-linear separability. We add a small uniform noise term to increase the complexity of the problem and with an 80-20 train-test split. We acknowledge the limitations of applicability of a synthetic dataset and therefore supplement our results using a real-world dataset of fraudulent credit card transactions (Le Borgne

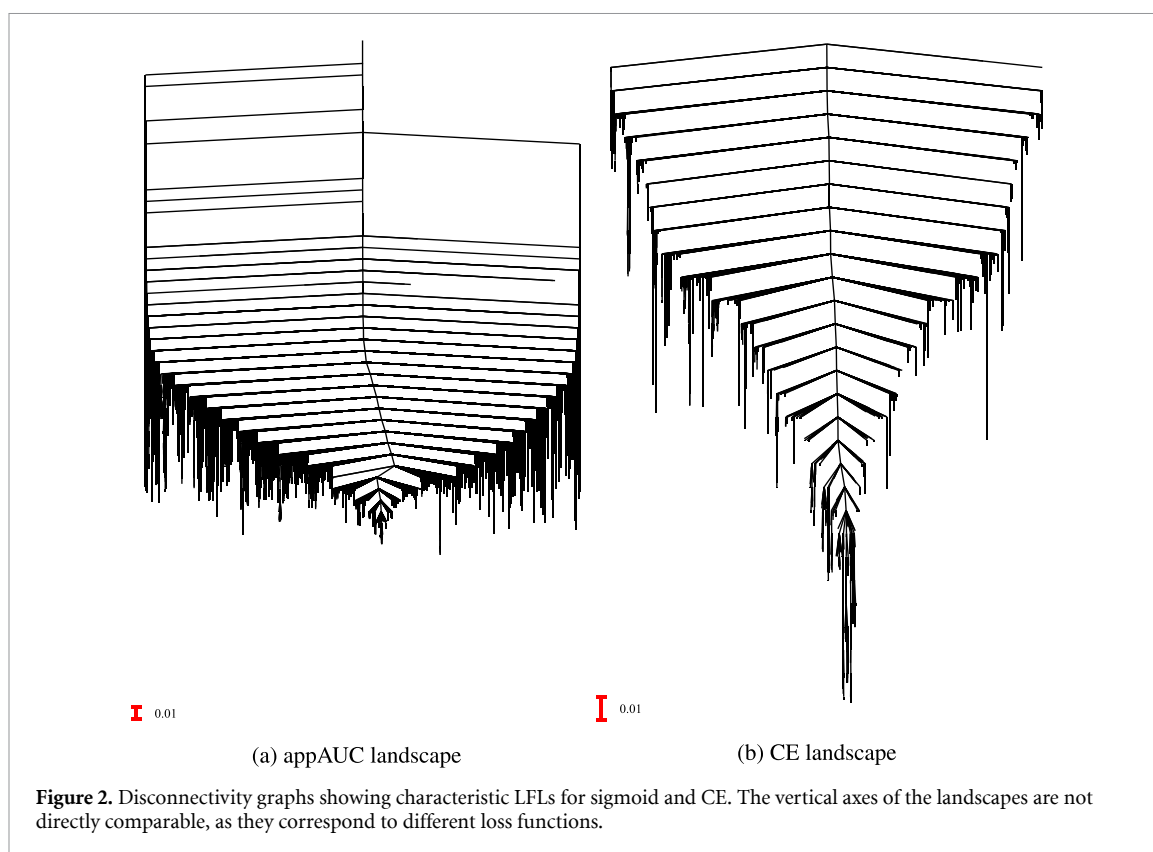


**Table 1.** Characteristic summary statistics for LFLs after exhaustive landscape exploration.

Loss function	# minima	AUC			# transition states	LPPHE	
		best	$\mu$	$\sigma$		$\mu$	$\sigma$
Sigmoid	13 948	0.81	0.7	0.04	25 957	-93	7.2
CE	1903	0.77	0.66	0.03	3606	-110	4.4

and Bontempi 2004). The dataset is highly imbalanced with only 10% of all datapoints classified as fraudulent transaction.

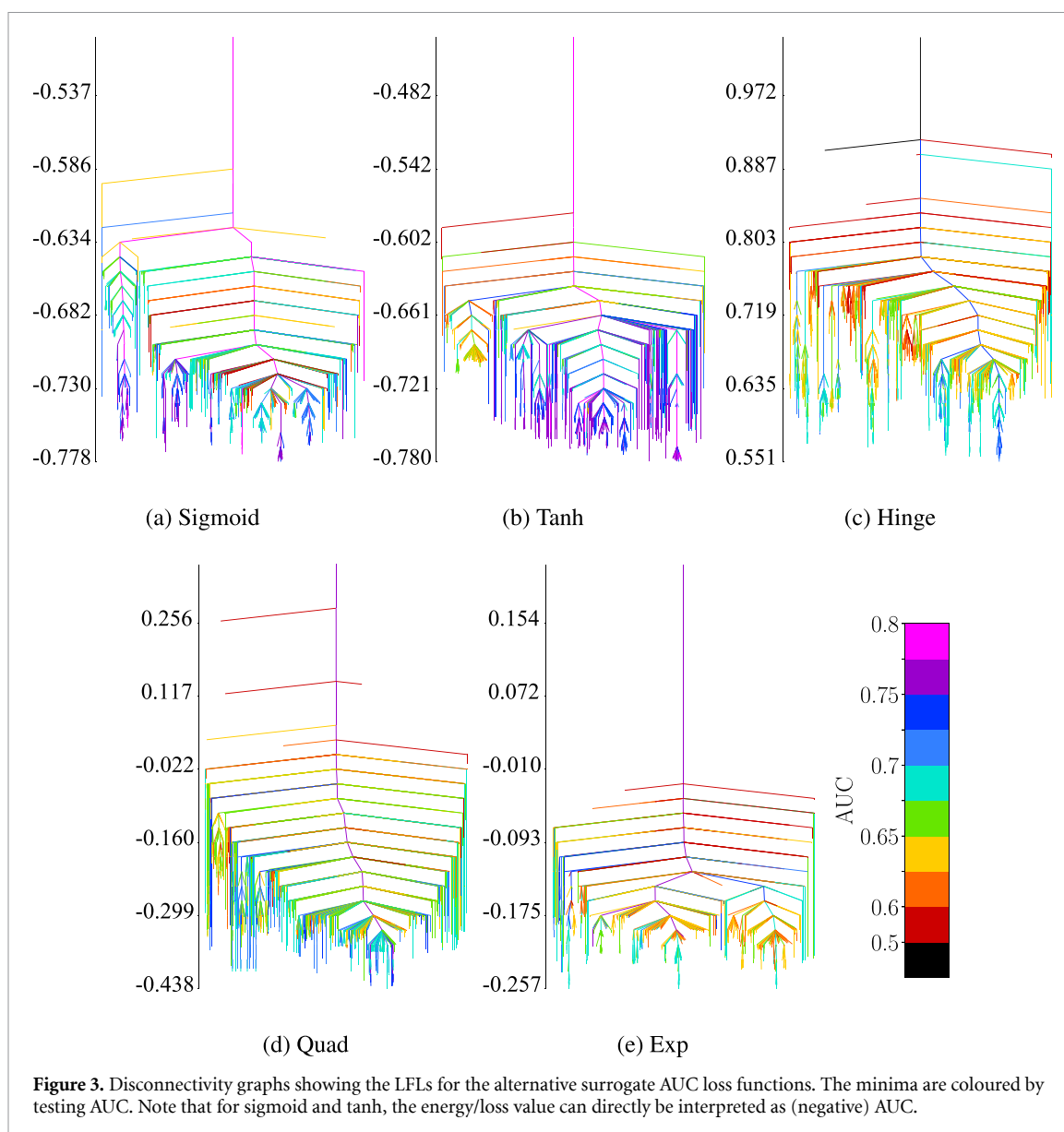
### 3. Results

In this section, we highlight three distinct points of interest. Firstly, we visualise and outline key differences between the AUC and CE landscapes. Secondly, we present an extended quantitative and geometric analysis of different AUC surrogates. Thirdly, we provide a comparison between minima of the AUC and CE landscape in terms of their classification properties.

#### 3.1. LFL properties

The loss function landscapes for AUC-approximated and CE loss functions look substantially different (figure 2). We performed landscape exploration using PATHSAMPLE until no new minima were found. For computational reasons, we only compare sigmoid appAUC with CE, and show below that for shorter timescales, sigmoid looks similar to the other surrogates. In particular, we find that the CE landscape is much more convex or funnelled than the appAUC landscape, with larger uphill barriers. In molecular science, this structure is associated with self-organising systems where relaxation to the global minimum is relatively efficient (Wales 2003).

In table 1 we report some summary statistics to characterise the two different LFLs numerically. The last column reports the mean of the log-product of positive Hessian Eigenvalues (LPPHE) for all minima of the landscape. This measure of basin geometry provides insight into the local curvature and hence the ‘flatness’ of a minimum (Verpoort *et al* 2020) and the volume of the corresponding basin of attraction (Mezey 1987, Wales 2003). The smaller the LPPHE, the flatter the local basin. Table 1 shows that the appAUC landscape



has substantially more minima and transition states than the CE landscape. Further, the mean LPPHE of all appAUC minima is larger than for the CE minima.

### 3.2. AUC surrogates

Table 2 shows a comparison of the different appAUC surrogates (section 2.3.1) after a week of landscape exploration. We find that these functions behave similarly, with comparable AUCs found and more minima than the CE landscape. The mean LPPHEs vary, the higher values belonging to the two functions that are true approximations to the stepwise AUC, namely sigmoid and tanh. They are all nonetheless larger or equal to the CE LFL in table 1. The disconnectivity graphs for these alternative appAUC functions are shown in figure 3. They are all similar to the appAUC landscape in figure 2 in the sense that they appear very wide (referred to as ‘glassy’ in molecular sciences) and much less single-funnelled than the CE LFL.

### 3.3. Loss-AUC correlation

Below, we show the correlation between loss value (energy) and AUC for test data for the different surrogate losses (figure 4). In all five cases, there is a significant negative correlation. Tanh has the most negative Pearson correlation coefficient of  $-0.83$ , followed by sigmoid and hinge.

### 3.4. appAUC minima in the CE LFL

Another point of interest is to understand the relationship between CE loss value and testing AUC for different LFLs. In figure 5 we use sigmoid to represent appAUC. We see that the negative correlation between

**Table 2.** Summary statistics for LFLs with alternative appAUC functions and CE as comparison.

Loss function	# minima	AUC			# transition states	LPPHE	
		Best	$\mu$	$\sigma$		$\mu$	$\sigma$
Sigmoid	4202	0.78	0.67	0.04	4264	-99	10
Hinge	6086	0.74	0.64	0.03	5822	-109	12
Tanh	3562	0.79	0.68	0.05	3000	-94	14
Quad	3606	0.77	0.65	0.04	3464	-103	11
Exp	2563	0.77	0.64	0.03	2515	-110	12

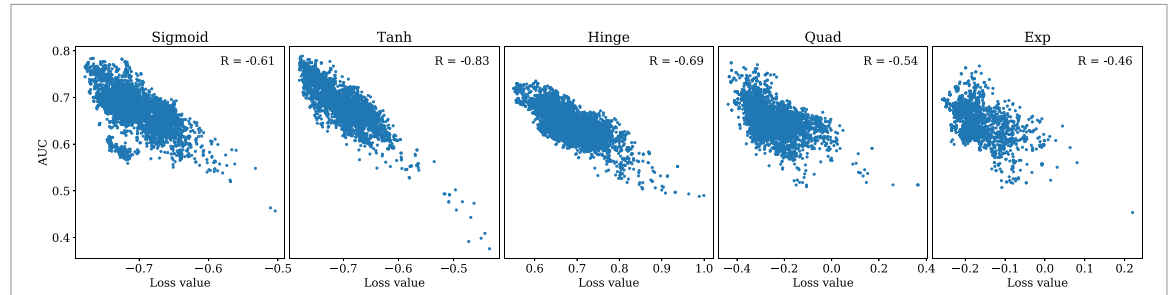


**Figure 4.** AUC vs loss correlation for the five different AUC surrogate functions. Minima at lower values of loss generally correspond to higher AUC values.

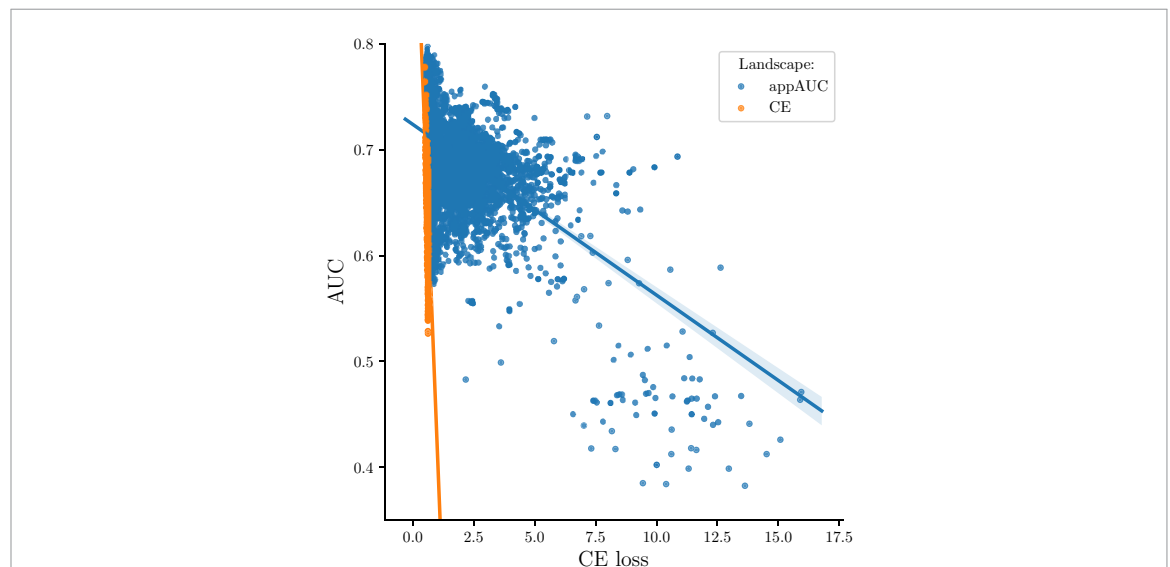


**Figure 5.** Correlation between CE loss and testing AUC for minima from CE and sigmoid LFLs.

CE loss and AUC is much stronger for minima of the CE than for the appAUC landscape. Hence, for most minima of the appAUC landscape, the CE loss values are relatively high, even though some of them may in fact have a higher AUC than the CE minima. This result raises the question of how good a diagnostic the CE loss is for the testing AUC. The insights into the position of appAUC minima within the CE LFL can be combined with the previous results on appAUC minima and the minimum they map to in the CE LFL. Above, we have identified that there exist many appAUC minima that are not minima of the CE LFL and thus have a higher CE loss value, but have comparable testing AUC. In general, while the best appAUC minima have reasonably low CE loss, the mean loss of 1.2 is nearly twice as high as for CE minima. The median of 0.8 is slightly lower, indicating a few very high loss minima, which lie in the lower right hand corner of figure 5.

**3.5. Credit card dataset**

We performed the same analysis on the imbalanced, real-world credit card dataset. Optimising AUC on such datasets is expected to be particularly useful, because the AUC as a measure is invariant to class imbalance. The appAUC landscape has more and better minima, and larger LPPHEs (table 3). As above, the CE landscape is single funnelled unlike the appAUC landscape, similar to figure 2.



**Table 3.** Summary statistics for credit card fraud LFLs.

Loss function	# minima	AUC			# transition states	LPPHE	
		Best	$\mu$	$\sigma$		$\mu$	$\sigma$
Sigmoid	3448	0.99	0.96	0.02	2343	-772	38
CE	1721	0.97	0.96	0.01	1584	-858	9

## 4. Discussion

We observe that the appAUC and CE LFLs have rather different characteristics, emphasising the point that alternative loss functions are truly different. In this section, we discuss and explain these observations, both empirically and theoretically. We explain why an analysis of the LFL can offer unique insights into the understanding of loss functions. Different characteristics of such a function may be important, and studying the LFL can help to choose an appropriate loss function. We also provide a comparison of the different AUC surrogates.

### 4.1. Comparison of loss function landscapes

As the disconnectivity graphs in figure 2 show, the CE landscape is more funnelled, and there are fewer minima. However, not only does the number of minima vary, the LPPHE also indicates that the minima appear rather different. Flatter minima (smaller LPPHE) are sometimes considered advantageous, because they may be more robust to perturbations in the weights (Hochreiter and Schmidhuber 1997), and therefore potentially also to noise in the training data. The increased robustness is explained by a lower deviation from the loss value of the global minimum for small deviations in training data or model hyperparameters in flatter landscapes where the gradients are small. This feature may constitute a geometrically-inspired argument against using the appAUC landscape if appAUC minima are less robust. The data suggest that on average the CE minima are relatively flat, which may translate to increased robustness to perturbations of the weights.

The location of appAUC minima within the CE LFL raises several new questions. Figure 5 illustrates the weakly negative correlation between CE loss and testing AUC for appAUC minima, much weaker than for CE LFL minima. This result initially seems intuitive, as we are looking at the CE LFL. The fact that the correlation between testing AUC and loss is more strongly negative for local minima of the CE loss function means that the CE loss works well for the minima in its own LFL. However, there also exist points in the CE LFL that are not minima (but minima of the appAUC) with higher loss and also higher AUC. Hence, under the assumption that appAUC is the more ‘accurate’ loss function, this analysis highlights some weaknesses of the CE LFL, namely not identifying some better, correct solutions. A mathematical foundation of the limitations of CE as opposed to appAUC is given in the next section.

### 4.2. Theoretical interpretation

To explain our empirical results, we can provide a theoretical basis for some of the observations. Notably, the substantially higher number of minima of the appAUC LFL is explained by mathematical properties of the solution space for CE in relation to appAUC loss generally. In fact, the solutions to CE loss are a subset of the solutions to the appAUC loss (Menon and Williamson 2016). The optimal solution of appAUC is any function that has a strictly monotonic relationship with  $P(y = 1|x)$  (Gao and Zhou 2015). On the other hand, the optimal solution of CE loss is  $P(y = 1|x)$ . Thus, a space of solutions for appAUC is infinitely larger than CE loss and therefore it should have more minima. The CE loss with Softmax belongs to the class of ‘strictly proper composite’ losses (Reid and Williamson 2010) which estimates  $P(y = 1|x)$ . In statistics, this is also referred to as ‘proper scoring rule’ (Buja *et al* 2005). Obviously,  $P(y = 1|x)$  has a strictly monotonic relationship with itself and hence must be optimal w.r.t. AUC, however this relationship must not hold the other way, optimising AUC must not necessarily be optimal w.r.t.  $P(y = 1|x)$ . Furthermore, the same line of argument also allows us to explain why appAUC minima are not necessarily close to CE minima in Euclidean space. Minimising appAUC does not give any additional incentive to find solutions of the kind  $P(y = 1|x)$  compared to any other solutions which may have a strictly monotonic relationship with  $P(y = 1|x)$ .

### 4.3. appAUC vs CE loss function

The appAUC landscape we have considered has approximately eight times as many minima as the corresponding CE landscape. The global minimum for appAUC achieves better testing AUC, and the mean AUC is also higher, yet there are also a few especially poor minima in the AUC landscape that are not found for the CE case. For practical applications the existence of solutions that are poor classifiers is probably not a

concern, because finding low-lying minima is relatively straightforward. However, computation of the appAUC as done here scales as  $\mathcal{O}(N^2)$ , where  $N$  is the number of data points, which is much more intensive than the  $\mathcal{O}(N)$  requirement associated with CE. Additionally, minima of the CE LFL seem to be more robust. In summary, exploiting the appAUC directly is more attractive if computational cost is not a problem, especially if the loss function landscape can be studied extensively. For machine learning applications involving large deep networks, where only a single minimum is identified, and where computational cost is a major concern, the CE landscape may be the best choice. This result strengthens the case for using CE as a ‘standard’ loss function, while also highlighting its limitations, and illustrating how using different loss functions can be beneficial.

#### 4.4. AUC surrogates

We observe that the LFLs for all AUC surrogates look roughly similar, and distinctly different from the CE LFL, providing a strong argument for a fundamental geometric difference between these loss functions that has not been shown before. We also observe that the hinge loss has substantially more minima than all other surrogates, yet the testing AUCs are much worse. This result may be explained by the fact that hinge is not AUC consistent, which means that the hinge functional space does not contain the AUC-optimal solution for this problem. Quad, tanh and sigmoid have broadly similar characteristics with small deviations in the LPPHE, while the exponential does slightly worse in terms of AUC but has very flat minima, similar to the CE landscape. Hence, using an exponential AUC surrogate may provide more robust solutions than other surrogates. However, if the main objective is to maximise testing AUC, tanh seems to be the best choice, as it not only has the highest AUC, but also the strongest inverse correlation between energy and AUC. Both tanh and sigmoid are directly approximating the stepwise AUC, which explains the strongly negative correlations, while both exponential and squared exponential function behave similarly as expected.

#### 4.5. Conclusions

Loss functions are essential to guide the learning process in neural networks. We have provided a detailed analysis of the approximate AUC landscape based on global exploration of tractable but realistic examples. In this contribution, we have proposed a new method to understand and select a loss function, based on geometric properties of the LFL. We have shown that LFLs for appAUC and the standard CE LFL are qualitatively and quantitatively different. We have also provided a detailed comparison of relevant LFL features between AUC surrogates and shown that the AUC-inconsistent hinge has much lower AUC than the other surrogates (but more minima) and that the exp surrogate has wide, robust minima, similar to the CE LFL. We find that optimising the AUC improves testing AUC, but CE minima have on average smaller LPPHEs, which may make them more robust. In general, we observe a tradeoff between robustness and testing AUC for all the loss functions. The greater computational cost of optimising the AUC directly is likely to be the main drawback of this approach. A quantitative analysis of geometric features of the LFL, such as by-minimum AUC, energy-testing AUC correlation, number of minima (landscape convexity), and LPPHE i.e. catchment basin volumes which are connected to minima robustness, provides insights into the strengths and weaknesses of loss functions. Hence, this analysis provides a valuable tool to guide loss function selection for machine learning applications.

### Data availability statement

No new data were created or analysed in this study.

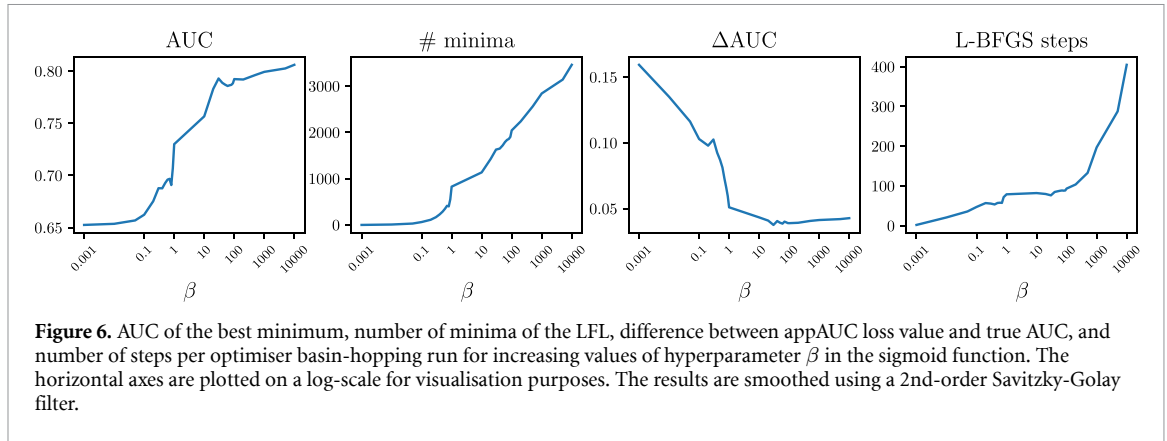
### Acknowledgments

M N acknowledges funding from Downing College, Cambridge and specifically the Voellm-Hruska PhD studentship. D J W and C T C gratefully acknowledge funding from the EPSRC. D J W gratefully acknowledges an International Chair at the Interdisciplinary Institute for Artificial Intelligence at 3iA Cote d’Azur, supported by the French government, reference ANR-19-P3IA-0002, which has provided interactions that furthered the present research project. We declare no competing interests.

### Appendix

#### A.1. Basin-hopping optimisation

Surveying the LFL for a neural network requires methods to locate minima of the landscape and connect them via transition states, defined as index one saddles (Murrell and Laidler 1968). We perform global



optimisation using the basin-hopping method, which uses a Metropolis criterion to avoid getting stuck in local minima (Li and Scheraga 1987, Wales and Doye 1997). For local minimisation we use a modified quasi-Newton L-BFGS (Limited-memory Broyden–Fletcher–Goldfarb–Shanno) algorithm (Nocedal 1980). After a local basin of attraction (local minimum) is found via L-BFGS optimisation, a ‘basin-hopping’ jump is performed to some other point in the LFL. This jump is always accepted if the energy, here loss value, is lower than the current minimum. If the loss value of the new point is higher, it is accepted with probability

$$P \propto \exp\left(-\frac{\Delta\tilde{E}}{k_B T}\right), \quad (8)$$

where  $\Delta\tilde{E}$  is the difference in loss value between the current minimum and the new point,  $k_B$  the Boltzmann constant and  $T$  a fictitious temperature. Intuitively, if the energy difference between the old and new points is large, the move is less likely to be accepted. A minimum is characterised as such if a RMS norm of gradient vector) convergence criterion at a threshold of  $10^{-10}$  is reached.

## A.2. Hyperparameter ablation study

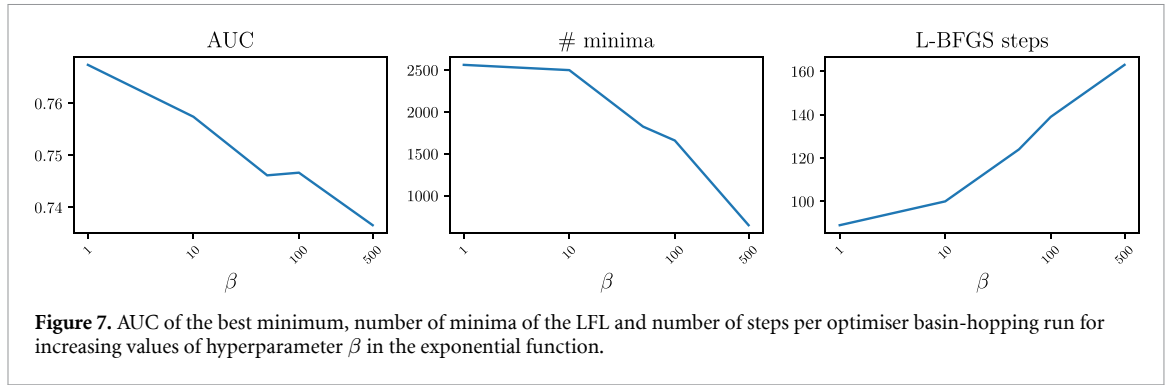
### A.2.1. Sigmoid

The relevant hyperparameter in the sigmoid function is  $\beta$  in the exponent (see equation (7)). For larger  $\beta$ , the function becomes more stepwise, i.e. a better approximation to the true AUC, with

$$\lim_{\beta \rightarrow \infty} \sigma(z; \beta) \rightarrow \Theta(z), \quad (9)$$

where again  $\sigma(z)$  denotes the sigmoid and  $\Theta(z)$  the Heaviside step function. We are interested in the impact of the hyperparameter  $\beta$  on the appAUC LFL. Figure 6 shows the effect on the loss function landscape of increasing  $\beta$  (on a log scale). Clearly, both the number of minima in the LFL and the AUC of the best minimum increase with  $\beta$ . The  $\Delta$ AUC plot in Figure 6 shows the median absolute difference between the approximate AUC value, i.e. the value of the loss function, and the true AUC, for all minima found at a specific  $\beta$ . This value is inversely proportional to  $\beta$  before it plateaus off at a median AUC difference of around 0.04. This median absolute difference is a relevant metric because it shows how closely the appAUC approximates the true AUC value. The rightmost plot in figure 6 shows a measure of the computational cost associated with optimising the appAUC loss function for different values of  $\beta$ . The number of optimisation steps for each iteration of the L-BFGS optimiser grows roughly linearly with  $\beta$ .

The difference between the true AUC and the approximated AUC is inversely proportional to  $\beta$ , as expected, because for larger  $\beta$ , the AUC approximation becomes more stepwise and hence more exact. We find that for  $\beta > 50$ , the median difference goes to around 0.04, which means it is a reasonably good approximation of the true AUC. We also observe an increase in best AUC, as well as the number of minima of the LFL with increasing  $\beta$ . All of these observations suggest that larger values of  $\beta$  are better, but increased performance comes at an increased computational cost. The reason for this increase is that the number of optimisation steps in the L-BFGS routine increases for larger  $\beta$ . Most likely, this result can be explained by the flatter appAUC function at large  $\beta$  around local minima. In flatter regions, convergence to a true minimum usually requires more optimisation steps because the function is more anharmonic. To conclude, we suggest a value for  $\beta$  of around 40. For higher values, the AUC does not improve significantly, while the computational cost, measured by the number of optimisation steps, increases linearly. Lastly, the distance between appAUC and CE minima for the number of optimisation steps, as opposed to Euclidean distance,



produces a larger tail in the plot due to the nature of the L-BFGS optimiser. The step size is determined by the L-BFGS formulation, and for a small step size there will be substantially more steps for the same Euclidean distance. We expect the number of steps to grow when the LFL is more locally anharmonic.

### A.2.2. Exponential

The same analysis is performed with the exponential surrogate function,  $\ell(z) = \exp(-\beta z)$ , in figure 7. Similar conclusions to the sigmoid function are drawn for L-BFGS optimiser steps. However, the number of minima found and the best AUC decrease with increasing  $\beta$ . Larger values of  $\beta$  here cause the exponential function to more closely resemble a step for  $z > 0$ , but the function does not then plateau for  $z < 0$  as nicely, which is perhaps the cause of the worse AUCs. It does not make sense to calculate  $\Delta AUC$  here, as  $\exp(-\beta z)$  does not truly attempt to ‘approximate’ the actual step-function AUC. From this analysis we conclude that  $\beta = 1$  is the best parameter to use for the exponential function.

### A.2.3. Regularisation parameter: $\lambda$

The  $\lambda W^2$  in equation (1) represents an L2 regularisation term, which eliminates zero Hessian Eigenvalues and counteracts overfitting. To pick a suitable value for  $\lambda$ , we study the effect of changes in  $\lambda$  on the topology of the LFL. Furthermore, we want to look into whether the effect of changes in  $\lambda$  are congruent between appAUC and CE LFL. We find that changing  $\lambda$  has similar effects across both appAUC and CE LFL. In both cases, decreasing  $\lambda$  by  $10^{-2}$  roughly doubles the computational cost. This supports results from previous work showing that landscapes with smaller  $\lambda$  contain more minima (figure 8) and are more costly to be optimised Mehta et al (2018). A landscape with larger  $\lambda$  is more convex and hence easier to optimise than systems with small  $\lambda$ . The topology of the LFL remains similar (CE more funnelled, appAUC much wider) across different  $\lambda$  (figure 8). Lastly, table 4 shows  $\lambda = 10^{-5}$  as a good balance between over- and underfitting, producing the highest testing AUCs. In conclusion, we decided on  $\lambda = 10^{-5}$  as a trade-off between computational cost and overfitting, while still presenting a characterisable landscape.

### A.3. Equality in equation (5)

The AUC is defined by the following integral:

$$AUC(\mathbf{W}; \mathbf{X}) = \int_0^1 T(\mathbf{W}; \mathbf{X}, P) dF(\mathbf{W}; \mathbf{X}, P). \tag{10}$$

Substituting in  $T$  and  $F$  (equations (2) and (3)) gives:

$$AUC(\mathbf{W}; \mathbf{X}) = \int_0^1 \frac{\sum_d \delta(c^d - 1) \Theta(p_1(\mathbf{W}; \mathbf{x}^d) - P)}{\sum_d \delta(c^d - 1)} d \left( \frac{\sum_{d'} (1 - \delta(c^{d'} - 1)) \Theta(p_1(\mathbf{W}; \mathbf{x}^{d'}) - P)}{\sum_{d'} 1 - \delta(c^{d'} - 1)} \right). \tag{11}$$

We may take outside of the integral any factors that do not depend on the parameter  $P$ . We note also that the sums  $\sum_d \delta(c^d - 1)$  and  $\sum_{d'} 1 - \delta(c^{d'} - 1)$  are simply  $N_p$  (the number of positive cases) and  $N_N$  (the number of negative cases), respectively, and that the sums in the numerator, reduce to taking the sum over all positive points, with  $d = p$ , and all negative points, with  $d' = n$ :

$$AUC(\mathbf{W}; \mathbf{X}) = \frac{1}{N_p N_N} \sum_p \sum_n \int_0^1 \Theta(p_1(\mathbf{W}; \mathbf{x}^p) - P) d\Theta(p_1(\mathbf{W}; \mathbf{x}^n) - P). \tag{12}$$

Because the parameter  $P$  is continuous, we can write:

$$d\Theta(p_1(\mathbf{W}; \mathbf{x}^n) - P) = -\delta(p_1(\mathbf{W}; \mathbf{x}^n) - P) dP. \tag{13}$$

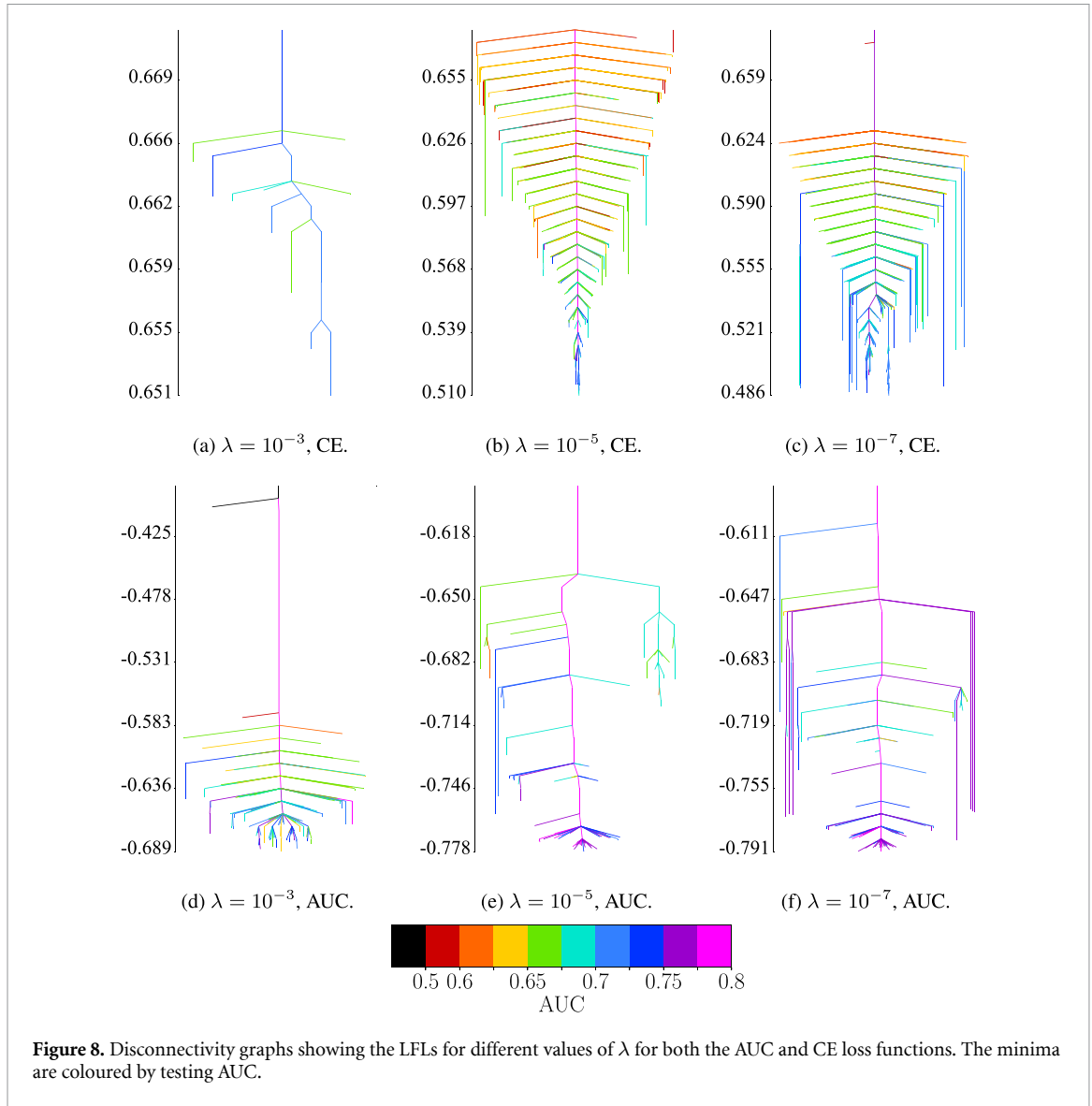


**Table 4.** Testing AUC for various values of  $\lambda$ .

$\lambda$	$10^{-1}$	$10^{-3}$	$10^{-5}$	$10^{-7}$	$10^{-9}$
appAUC	0.66	0.78	0.79	0.79	0.72
CE	0.5	0.73	0.77	0.74	0.71

The limits of the integral must be changed: when  $P = 1, \Theta = 0$  and when  $P = 0, \Theta = 1$ , so  $\int_0^1 \rightarrow \int_1^0$  or  $-\int_0^1$ :

$$AUC(\mathbf{W}; \mathbf{X}) = \frac{1}{N_p N_N} \sum_p \sum_n \int_0^1 \Theta(p_1(\mathbf{W}; \mathbf{x}^p) - P) \delta(p_1(\mathbf{W}; \mathbf{x}^n) - P) dP. \quad (14)$$

Finally, we integrate over this  $\delta$ -function, using the property  $\int f(x)\delta(x - x_0) dx = f(x_0)$ , to obtain equation (5):

$$AUC(\mathbf{W}; \mathbf{X}) = \frac{1}{N_p N_N} \sum_p \sum_n \Theta(p_1(\mathbf{W}; \mathbf{x}^p) - p_1(\mathbf{W}; \mathbf{x}^n)). \quad (15)$$

Note that the minus sign has disappeared, because the integral limits were exchanged.

#### A.4. Derivatives

Equation (6) can now be differentiated and treated as a function that can be optimised, just like equation (1). For completeness and comparison, the first and second derivatives of both equations (1) and (6) are given.

For compactness, the arguments of each function are omitted, but a superscript is given if the function depends on a specific data point:

$$p_{c^d}(\mathbf{W}; \mathbf{x}^d) \rightarrow p_{c^d}^d, \quad \sigma(p_1^p - p_1^n) \rightarrow \sigma^{p:n}. \tag{16}$$

Finally, the derivatives are given in component form (e.g.  $\partial \text{CE} / \partial \mathbf{W}$  is a vector of length  $N_w$ , the number of weights), with labels  $\mu, \nu, \dots$  denoting the relevant parts of the weight vector,  $\mathbf{W}$ .

The loss function:

$$\text{CE} = -\frac{1}{N} \sum_{d=1}^N \ln(p_{c^d}^d) + \lambda \mathbf{W}^2, \tag{17}$$

$$\frac{\partial \text{CE}}{\partial w_\mu} = -\frac{1}{N} \sum_{d=1}^N \frac{1}{p_{c^d}^d} \frac{\partial p_{c^d}^d}{\partial w_\mu} + 2\lambda w_\mu, \tag{18}$$

$$\frac{\partial^2 \text{CE}}{\partial w_\mu \partial w_\nu} = -\frac{1}{N} \sum_{d=1}^N \left( \frac{1}{p_{c^d}^d} \frac{\partial^2 p_{c^d}^d}{\partial w_\mu \partial w_\nu} - \frac{1}{(p_{c^d}^d)^2} \frac{\partial p_{c^d}^d}{\partial w_\mu} \frac{\partial p_{c^d}^d}{\partial w_\nu} \right) + 2\lambda \delta_{\mu\nu}. \tag{19}$$

The approximate AUC function (note an L2 regularisation term has been added, to combat overfitting):

$$A = \frac{1}{N_p N_N} \sum_p \sum_n \sigma^{p:n} + \lambda \mathbf{W}^2, \tag{20}$$

$$\frac{\partial A}{\partial w_\mu} = \frac{1}{N_p N_N} \sum_p \sum_n \left[ \beta \sigma^{p:n} (1 - \sigma^{p:n}) \left( \frac{\partial p_1^p}{\partial w_\mu} - \frac{\partial p_1^n}{\partial w_\mu} \right) \right] + 2\lambda w_\mu, \tag{21}$$

$$\begin{aligned} \frac{\partial^2 A}{\partial w_\mu \partial w_\nu} = \frac{1}{N_p N_N} \sum_p \sum_n \left[ \beta^2 \sigma^{p:n} (1 - \sigma^{p:n}) (1 - 2\sigma^{p:n}) \left( \frac{\partial p_1^p}{\partial w_\mu} - \frac{\partial p_1^n}{\partial w_\mu} \right) \left( \frac{\partial p_1^p}{\partial w_\nu} - \frac{\partial p_1^n}{\partial w_\nu} \right) \right. \\ \left. + \beta \sigma^{p:n} (1 - \sigma^{p:n}) \left( \frac{\partial^2 p_1^p}{\partial w_\mu \partial w_\nu} - \frac{\partial^2 p_1^n}{\partial w_\mu \partial w_\nu} \right) \right] + 2\lambda \delta_{\mu\nu}. \end{aligned} \tag{22}$$

Finally, for both the loss function and approximate AUC function, the derivatives of  $p_\ell^d$  must be evaluated ( $\ell$  is a placeholder label to cover both cases,  $c^d$  or 1). Here we separate the four different groups of weights. These groups are: input-hidden weights (denoted as  $w^{(2)}$ ), hidden-output ( $w^{(1)}$ ), bias to hidden nodes ( $w^{bh}$ ) and bias to output nodes ( $w^{bo}$ ).

First derivatives:

$$\frac{\partial p_\ell^d}{\partial w_\mu^{bo}} = p_\ell^d \Delta_{\ell\mu}^d, \tag{23}$$

$$\frac{\partial p_\ell^d}{\partial w_\mu^{bh}} = (s_\mu^d)^2 \sum_{i=1}^C w_{i\mu}^{(1)} \frac{\partial p_\ell^d}{\partial w_i^{bo}}, \tag{24}$$

$$\frac{\partial p_\ell^d}{\partial w_{\mu\nu}^{(1)}} = t_\nu^d \frac{\partial p_\ell^d}{\partial w_\mu^{bo}}, \tag{25}$$

$$\frac{\partial p_\ell^d}{\partial w_{\mu\nu}^{(2)}} = x_\nu^d \frac{\partial p_\ell^d}{\partial w_\mu^{bh}}, \tag{26}$$

where

$$t_\nu^d \equiv \tanh \left( w_\nu^{bh} + \sum_{k=1}^{N_{in}} w_{\nu k}^{(2)} x_k^d \right) \quad s_\nu^d \equiv \text{sech} \left( w_\nu^{bh} + \sum_{k=1}^{N_{in}} w_{\nu k}^{(2)} x_k^d \right), \tag{27}$$

and

$$\Delta_{ij}^d \equiv \delta_{ij} - p_j^d. \tag{28}$$

Second derivatives:

$$\frac{\partial^2 P_\ell^d}{\partial w_{\mu}^{\text{bo}} \partial w_{\rho}^{\text{bo}}} = P_\ell^d (\Delta_{\ell\rho}^d \Delta_{\ell\mu}^d - P_\mu^d \Delta_{\mu\rho}^d), \quad (29)$$

$$\frac{\partial^2 P_\ell^d}{\partial w_{\mu}^{\text{bh}} \partial w_{\rho}^{\text{bo}}} = (s_\mu^d)^2 \sum_{i=1}^C w_{i\mu}^{(1)} \frac{\partial^2 P_\ell^d}{\partial w_i^{\text{bo}} \partial w_{\rho}^{\text{bo}}}, \quad (30)$$

$$\begin{aligned} \frac{\partial^2 P_\ell^d}{\partial w_{\mu}^{\text{bh}} \partial w_{\rho}^{\text{bh}}} = & \left[ (s_\rho^d)^2 \sum_{i,j=1}^C w_{i\mu}^{(1)} w_{j\rho}^{(1)} \frac{\partial^2 P_\ell^d}{\partial w_i^{\text{bo}} \partial w_j^{\text{bo}}} \right. \\ & \left. - 2\delta_{\mu\rho} t_\mu^d P_\ell^d \sum_{i=1}^C w_{i\mu}^{(1)} \Delta_{\ell i}^d \right] \times (s_\mu^d)^2, \end{aligned} \quad (31)$$

$$\frac{\partial^2 P_\ell^d}{\partial w_{\mu\nu}^{(1)} \partial w_{\rho}^{\text{bh}}} = t_\nu^d \frac{\partial^2 P_\ell^d}{\partial w_{\rho}^{\text{bh}} \partial w_{\mu}^{\text{bo}}} + \delta_{\nu\rho} P_\ell^d (s_\rho^d)^2 \Delta_{\ell\mu}^d, \quad (32)$$

$$\frac{\partial^2 P_\ell^d}{\partial w_{\mu\nu}^{(1)} \partial w_{\rho}^{\text{bo}}} = t_\nu^d \frac{\partial^2 P_\ell^d}{\partial w_{\mu}^{\text{bo}} \partial w_{\rho}^{\text{bo}}}, \quad (33)$$

$$\frac{\partial^2 P_\ell^d}{\partial w_{\mu\nu}^{(1)} \partial w_{\rho\sigma}^{(1)}} = t_\nu^d t_\sigma^d \frac{\partial^2 P_\ell^d}{\partial w_{\mu}^{\text{bo}} \partial w_{\rho}^{\text{bo}}}, \quad (34)$$

$$\frac{\partial^2 P_\ell^d}{\partial w_{\mu\nu}^{(2)} \partial w_{\rho}^{\text{bo}}} = x_\nu^d \frac{\partial^2 P_\ell^d}{\partial w_{\mu}^{\text{bh}} \partial w_{\rho}^{\text{bo}}}, \quad (35)$$

$$\frac{\partial^2 P_\ell^d}{\partial w_{\mu\nu}^{(2)} \partial w_{\rho}^{\text{bh}}} = x_\nu^d \frac{\partial^2 P_\ell^d}{\partial w_{\mu}^{\text{bh}} \partial w_{\rho}^{\text{bh}}}, \quad (36)$$

$$\frac{\partial^2 P_\ell^d}{\partial w_{\mu\nu}^{(2)} \partial w_{\rho\sigma}^{(1)}} = x_\nu^d \frac{\partial^2 P_\ell^d}{\partial w_{\rho\sigma}^{(1)} \partial w_{\mu}^{\text{bh}}}, \quad (37)$$

$$\frac{\partial^2 P_\ell^d}{\partial w_{\mu\nu}^{(2)} \partial w_{\rho\sigma}^{(2)}} = x_\sigma^d \frac{\partial^2 P_\ell^d}{\partial w_{\mu\nu}^{(2)} \partial w_{\rho}^{\text{bh}}}. \quad (38)$$

## ORCID iDs

Maximilian P Niroomand  <https://orcid.org/0000-0002-7189-0456>

David J Wales  <https://orcid.org/0000-0002-3555-6645>

## References

- Agarwal S 2014 Surrogate regret bounds for bipartite ranking via strongly proper losses *J. Mach. Learn. Res.* **15** 1653–74
- Baldassi C, Pittorino F and Zecchina R 2020 Shaping the learning landscape in neural networks around wide flat minima *Proc. Natl Acad. Sci.* **117** 161–70
- Ballard A J, Das R, Martiniani S, Mehta D, Sagun L, Stevenson J D and Wales D J 2017 Energy landscapes for machine learning *Phys. Chem. Chem. Phys.* **19** 12585–603
- Becker O M and Karplus M 1997 The topology of multidimensional potential energy surfaces: theory and application to peptide structure and kinetics *J. Chem. Phys.* **106** 1495–517
- Buja A, Stuetzle W and Shen Y 2005 Loss functions for binary class probability estimation and classification: structure and applications *Work. Draft* **3** 5–7
- Calders T and Jaroszewicz S 2007 Efficient AUC optimization for classification *Conf. on Principles of Data Mining and Knowledge Discovery* (Springer) pp 42–53
- Charoenphakdee N, Lee J and Sugiyama M 2019 On symmetric losses for learning from corrupted labels *Int. Conf. on Machine Learning* (PMLR) pp 961–70
- Chaudhari P, Choromanska A, Soatto S, LeCun Y, Baldassi C, Borgs C, Chayes J, Sagun L and Zecchina R 2019 Entropy-sgd: Biasing gradient descent into wide valleys *J. Stat. Mech.* **2019** 124018
- Cooper Y 2018 The loss landscape of overparameterized neural networks (arXiv:1804.10200)
- Cortes C and Mohri M 2004 AUC optimization vs. error rate minimization *Adv. Neural Inf. Process. Syst.* **16** 313–20
- Fort S and Scherlis A 2019 The goldilocks zone: towards better understanding of neural network loss landscapes *Proc. Conf. Artif. Intell.* **33** 3574–81

- Gao W and Zhou Z-H 2015 On the consistency of AUC pairwise optimization *Twenty-Fourth Int. Conf. on Artificial Intelligence*
- Ghanbari H and Scheinberg K 2018 Directly and efficiently optimizing prediction error and AUC of linear classifiers (arXiv:1802.02535)
- Hao Li, Zheng X, Taylor G, Studer C, and Goldstein T 2017 Visualizing the loss landscape of neural nets *arXiv preprint* (arXiv:1712.09913)
- Hastie T, Tibshirani R and Friedman J 2009 *The Elements of Statistical Learning* (New York: Springer)
- Henkelman G and Harnes J 2000 Improved tangent estimate in the nudged elastic band method for finding minimum energy paths and saddle points *J. Chem. Phys.* **113** 9978–85
- Henkelman G, Uberuaga B P and Jónsson H 2000 A climbing image nudged elastic band method for finding saddle points and minimum energy paths *J. Chem. Phys.* **113** 9901–4
- Hochreiter S and Schmidhuber J 1997 Flat minima *Neural Comput.* **9** 1–42
- Janocha K and Czarnecki W M 2017 On loss functions for deep neural networks in classification (arXiv:1702.05659)
- Lang K J and Witbrock M J 1988 Learning to tell two spirals apart *Proc. 1988 Connectionist Models Summer School* (San Mateo) pp 52–59
- Le Borgne Y-A and Bontempi G 2004 Machine learning for credit card fraud detection-practical handbook *ACM SIGKDD Explor. Newsl.* **6** 1–6
- Li Z and Scheraga H A 1987 Monte Carlo-minimization approach to the multiple-minima problem in protein folding *Proc. Natl Acad. Sci.* **84** 6611–15
- Martiniani S, Schrenk K J, Stevenson J D, Wales D J, and Frenkel D 2016 Turning intractable counting into sampling: computing the configurational entropy of three-dimensional jammed packings. *Phys. Rev. E* **93** 012906
- Mehta D, Zhao X, Bernal E A and Wales D J 2018 Loss surface of XOR artificial neural networks *Phys. Rev. E* **97** 052307
- Menon A K and Elkan C 2011 Link prediction via matrix factorization *Joint European Conf. on Machine Learning and Knowledge Discovery in Databases* (Springer) pp 437–52
- Menon A K and Williamson R C 2016 Bipartite ranking: a risk-theoretic perspective *J. Mach. Learn. Res.* **17** 6766–867
- Mezey P G 1987 *Potential Energy Hypersurfaces* (Amsterdam: Elsevier)
- Munro L J and Wales D J 1999 Defect migration in crystalline silicon *Phys. Rev. B* **59** 3969–80
- Murrell J N and Laidler K J 1968 Symmetries of activated complexes *Trans. Faraday Soc.* **64** 371–7
- Nocedal J 1980 Updating quasi-Newton matrices with limited storage *Math. Comput.* **35** 773
- Reid M D and Williamson R C 2010 Composite binary losses *J. Mach. Learn. Res.* **11** 2387–422
- Rosasco L, Vito E D, Caponnetto A, Piana M and Verri A 2004 Are loss functions all the same? *Neural Comput.* **16** 1063–76
- Trygubenko S A and Wales D J 2004a Analysis of cooperativity and localization for atomic rearrangements *J. Chem. Phys.* **121** 6689–97
- Trygubenko S A and Wales D J 2004b A doubly nudged elastic band method for finding transition states *J. Chem. Phys.* **120** 2082–94
- Verpoort P C et al 2020 Archetypal landscapes for deep neural networks *Proc. Natl Acad. Sci.* **117** 21857–64
- Wales D J 1997 GMIN: a program for basin-hopping global optimisation, basin-sampling, and parallel tempering
- Wales D J 2003 *Energy Landscapes* (Cambridge: Cambridge University Press)
- Wales D J 2003 OPTIM: a program for geometry optimisation and pathway calculations
- Wales D J 2003 PATHSAMPLE: a program for generating connected stationary point databases and extracting global kinetics
- Wales D J 2013 Surveying a complex potential energy landscape: overcoming broken ergodicity using basin-sampling *Chem. Phys. Lett.* **584** 1–9
- Wales D J and Doye J P K 1997 Global Optimization by Basin-Hopping and the lowest energy structures of Lennard-Jones clusters containing up to 110 atoms *J. Phys. Chem. A* **101** 5111–16
- Wales D J, Miller M A and Walsh T R 1998 Archetypal energy landscapes *Nature* **394** 758–60
- Yan L, Dodier R H, Mozer M and Wolniewicz R H 2003 Optimizing classifier performance via an approximation to the Wilcoxon-Mann-Whitney statistic *Proc. 20th International Conf. on Machine Learning (Icml-03)* pp 848–55
- Zeng Y, Xiao P and Henkelman G 2014 Unification of algorithms for minimum mode optimization *J. Chem. Phys.* **140** 044115